공학석사학위논문

분산 제약하에서 원격 제어되는 다수의 논홀로노믹 이동형 로봇의 대형 재구성 제어

Formation Reconfiguration Control of Multiple Teleoperated Nonholonomic Wheeled Mobile Robots under Distribution Constraint

2019 년 2 월

서울대학교 대학원

기계항공공학부

권 성 진

분산 제약하에서 원격 제어되는 다수의 논홀로노믹 이동형 로봇의 대형 재구성 제어

Formation Reconfiguration Control of Multiple Teleoperated Nonholonomic Wheeled Mobile Robots under Distribution Constraint

지도교수 이 동 준

이 논문을 공학석사 학위논문으로 제출함

2018 년 10 월

서울대학교 대학원

기계항공공학부

권 성 진

권성진의 공학석사 학위논문을 인준함

2018 년 12 월

위 원 장 박 종 우 (인)

부위원장 이 동 준 (인)

위 원 강 연 준 (인)

Abstract

Formation Reconfiguration Control of Multiple Teleoperated Nonholonomic Wheeled Mobile Robots under Distribution Constraint

Seongjin Kwon
Mechanical & Aerospace Engineering
The Graduate School
Seoul National University

We propose a novel framework for formation reconfiguration of multiple nonholonomic wheeled mobile robots (WMRs) in the changing driving environment. We utilize an onboard system of WMRs with the capability of sensing and computing. Each WMR has the same computing power for visualizing the driving environment, handling the sensing information and calculating the control action. One of the WMRs is the leader with the FPV camera and SLAM, while others with monocular cameras with limited FoV, as the followers, keep a certain desired formation during driving in a distributed manner. We set two control objectives, one is group driving and the other is holding the shape of the formation. We have to capture the control objectives separately and simultaneously, we make the best use of nonholonomic passive decomposition to split the WMRs' kinematics into those of the formation maintaining and group driving. The repulsive potential function to prevent the collision among WMRs and attractive potential function to restrict the boundary of follower WMRs' moving space due to limited FoV range of the monocular cameras while switching their formation

are also used. Simulation with 39 tanks and experiments with three WMRs are also performed to verify the proposed framework.

Keywords: Formation Reconfiguration, Nonholonomic Wheeled Mobile Robots, Passive Decompostiion, Teleoperation

Student Number: *2017-22264*

Acknowledgements

군문에 들어선지 어언 10년, 운 좋게 국가로부터 기회를 부여 받아 대한민국 최고의 대학에서 석사 과정을 밟을 수 있었습니다. 학부 때 전공했던 분야도 아니었거니와 우리나라에서 가장 높은 지식 수준을 자랑하는 곳에서의 시간이 될 것이었기에 기대감보다는 걱정이 먼저 앞섰습니다. 하지만 따뜻한 사람들을 만나게 되었고 제가 어려워 하는 일을 자신의 것인 듯 물심양면으로 도와주는 그들이 있었기에 무사히 2년여의 시간을 보낼 수 있었던 것 같습니다.

가장 먼저 군 위탁생이 생소하기도 하고 어찌보면 모험적일 수 있었음에도 불구하고 군에 대한 긍정적인 시각을 갖고 국방에 염려를 쏟아주시며 저를 선발, 지금 이 시간까지 끌어주신 이동준 교수님께 무한한 감사의 말씀을 드립니다. 꾸준한 가르침 덕택에 연구자로서의 유아기를 무사히 보내고 좋은 연구를 할 수 있는 방법과 그를 대할 때의 자세를 알게 되었습니다. 앞으로도 군인이자 학자로서의 길을 걸어가게 될 저에게 있어서 엄청난 자양분이 되었고 이는 앞으로 스스로 해낼 수 있는 성장기를 거쳐 진정한 학자가 될 수 있는 지표가 될 것입니다.

길다면 길고 짧다면 짧은 시간동안 함께 고생했던 INRoL 연구원 동료들에게도 감사의 말씀 전합니다. 연구의 성과를 여러분 덕분에 이루었을 뿐만 아니라 저라는 한 사람이 살아오면서, 또 앞으로 살아가면서 항상 최고의 가치로 생각할 인간관계를 훌륭한 사람들과 맺었다는 것 자체만으로도 크나큰 영광으로 생각합니다. 여러분들에게는 많이 생소할 수도 있는 군인이라는 특이한 신분을 가진 저를 낯설게만 생각하고 멀리할 수 있었을텐데 그렇지 않고 가까이 다가와 부족한 부분을 채워주고 같이 웃어주었기에 저도 걱정을 접고 스스럼 없이 그저 동일한 조직에 속한 구성원으로 녹아들 수 있었던 것 같습니다.

마지막으로 멀리서나마 항상 응원해주신 양가 부모님, 형님, 두 딸아이를 키우며 희생으로 내조해준 아내, 행복함과 즐거움만 주는 두 딸아이에게 감사드리며 더 발전하고 성장하는 모습으로 보답하겠습니다.

2019년 1월

권성진

Contents

List of Figures

Abbreviations

WMR	**W**heeled **M**obile **R**otbot
SLAM	**S**imultaneous **L**ocalization **A**nd **M**apping
FPV	**F**irst-**P**erson **V**iew
FoV	**F**ield **o**f **V**iew
LiDAR	**L**ight **D**etection **A**nd **R**anging
MCS	**M**ain **C**ontrol **S**tation
EKF	**E**xtended **K**alman **F**ilter
IMU	**I**nertial **M**easurement **U**nit
DoF	**D**egree **o**f **F**reedom

Chapter 1

Introduction

Multiple nonholonomic WMRs in the distributed system can be used for many tasks such as transporting materials and goods, exploring a specific area, driving in a group, and even in military operation by the merits of the system stated in [1]. However, the tasks are usually performed in unknown places, it is hard to grasp the whole driving environment. Moreover, there may be several types of terrain and obstacles that distrub the maneuver of robots. So, to operate the system more effectively, it is important to change the formation of WMRs [2] in according to various uncharactered situations.

In this thesis, we consider the problem when the WMRs switch their formation, especially from line graph topology [3] to triangular graph topology [4] and from triangular graph topology to line graph topology while changing the order of

WMRs. Here, the reason why we change the order of WMRs is related to military operation. Military equipments may often have to change their formation and even order of them situationally. We postulate the WMRs as the military equipments. In Fig. 1.1, there is the image of the system configuration we use. The system consists of: 1) one WMR, as a leader, has a LiDAR (light detection and ranging) sensor to know its own pose and capture the information of the driving environment in real time, a FPV (first-person view) camera to recognize the front conditions, computing power to calculate its control action and also to run SLAM (simultaneous localization and mapping) and communication capability with a following WMR (or following WMRs) and the MCS (master control station); and 2) two follower WMRs, each equipped with a monocular camera to measure the relative distance and pose from its following target WMR, and computing power for its control input and communicate with its target/following WMR.

When we operate these distributed WMRs in an unknown or an uncharactered environment, it is very difficult to carry out desired missions in a fully-autonomous manner. To escape such difficulties of the fully-autonomous operation, in this thesis, we utilize the latest teleoperation technique of one of the previous studies, the foundation of this thesis [1]. Even though [1] proposes the idea of triangular formation shape, it is confined to simulation, so we propose new algorithm for changing formation and implement the idea with three WMRs in Fig. 1.1. We utilize and extend the nonholonomic passive decomposition [5],

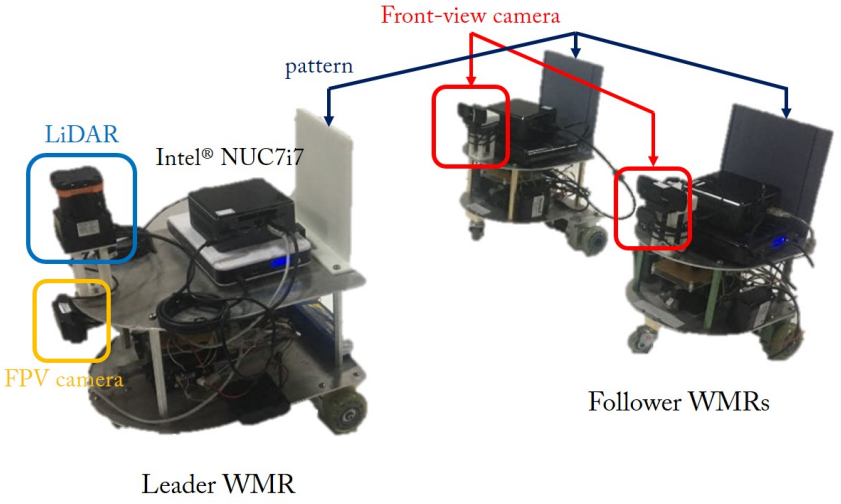

FIGURE 1.1: Distributed nonholonomic WMRs: one leader and two followers

[6], [7], [8] to split the group kinematics of the multiple WMRs into the inter-WMR formation aspect and their group driving aspect while fully respecting the nonholonomic constraint and the control/communication distribution requirement. We also apply repulsive potential function [9], [10] to avoid the collision of WMRs and attractive potential function [11], [12] to keep the view of cameras of follower WMRs facing the pattern of fore-running WMR.

Many techniques have been proposed for the control of multiple distributed nonholonomic WMRs, some demonstrated with on-board sensing and estimation [13], [14]. Many results have been reported for the teleoperation of distributed multiple mobile robots [15], [16]. Studies for the formation reconfiguration of nonholonomic wheeled mobile robots have been also carried out [2], [17], [18]. Yet,

to our knowledge, there has been no result so far, which systematically utilizes the formation reconfiguration control of the multiple teleoperated nonholonomic wheeled mobile robots under distribution constraint. The holistic framework for the distributed robot teleoperation with the onboard system, switching the formation is proposed in this thesis for the first time.

The rest of the thesis is organized as follows. The formation reconfiguration control design to achieve the proposed goal of this thesis and simulation result are presented in Sec. 2; Estimation and predictive display for the control and teleoperation are in Sec. 3; Experiments to demonstrate proposed framework is in Sec. 4; Conclude this thesis in Sec. 5.

Chapter 2

Formation Reconfiguration Control Design

2.1 Nonholonomic Passive Decomposition

Here, our goal is to design the control action for the WMRs maintaining the desired formation (i.e., line graph topology, triangular graph topology) without reference to the user command while moving through the user command with fully respecting the nonholonomic constraint. We consider the kinematics of WMRs without considering the slip effect and drifts of the wheel becuase the moving speed of WMRs is slow enough to neglect them.

We denote $j = 1$ is the leader WMR and $j = 2, ..., n$ for the follower WMRs. We define the configuration of the pair of the $j-$th and $(j+1)-$th WMRs by

$$q_{j,j+1} := [x_j; y_j; \phi_j; x_{j+1}; y_{j+1}; \phi_{j+1}] \in \Re^6$$

with their no-slip/drift conditions given by the Pfaffian constraint:

$$A_{j,j+1}\dot{q}_{j,j+1} = 0 \tag{2.1}$$

with $A_{j,j+1}\dot{q}_{j_j+1} := diag[A_j(q_j), A_{j+1}(q_{j+1})] \in \Re^{2\times 6}$ with $A_j(q_j) := \begin{bmatrix}\sin\phi_j & -\cos\phi_j & 0\end{bmatrix} \in \Re^{1\times 3}$, which is well-known to be completely nonholonomic.

The unconstrained distribution $\mathcal{D}^{\top}_{j,j+1}(q)$, which is the sub-space of the velocity respecting the nonholonomic constraint 2.1, can then be written by

$$\mathcal{D}^{\top}_{j,j+1} := \begin{bmatrix} c\phi_j & s\phi_j & 0 & 0 & 0 & 0 \\ 0 & 0 & 1 & 0 & 0 & 0 \\ 0 & 0 & 0 & c\phi_{j+1} & s\phi_{j+1} & 0 \\ 0 & 0 & 0 & 0 & 0 & 1 \end{bmatrix}$$

where $c\phi_j := \cos\phi_j$ and $s\phi_j := \sin\phi_j$. $\mathcal{D}^{\top}_{j,j+1}$ identifies the null-space of $A_{j,j+1} \in \Re^{2\times 6}$ in 2.1. We then can derive the drift-less nonlinear control equation of the two WMRs:

$$\dot{q}_{j,j+1} = \mathcal{D}^{\top}_{j,j+1}u_{j,j+1} \tag{2.2}$$

where $u_{j,j+1} := [v_j; w_j; v_{j+1}; w_{j+1}] \in \Re^4$ is the control input, with $v_j, w_j \in \Re$

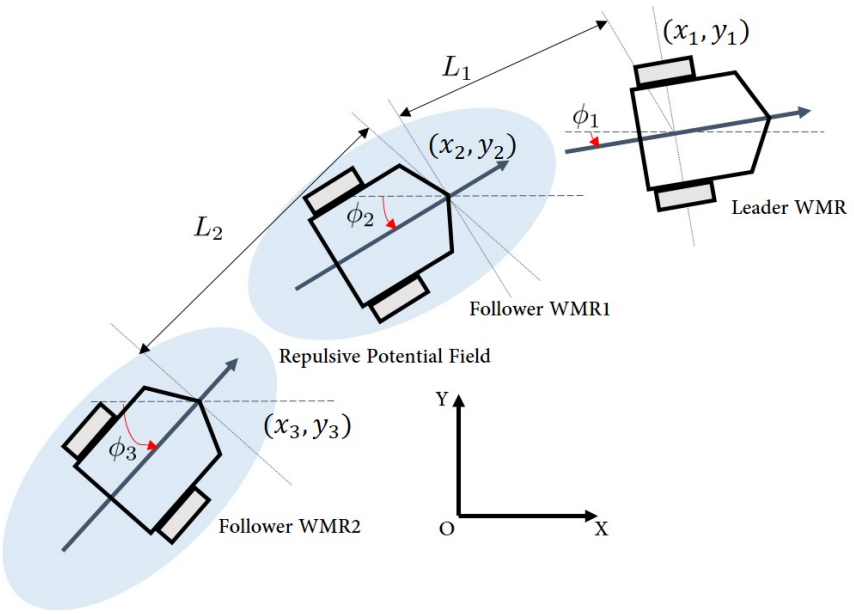

FIGURE 2.1: Geometry of distributed nonholonomic WMRs with repulsive potential field

being the forward and angular velocity commands of the j-th WMR. According to the previous study [1] , the control objective can be written by the following virtual constraint:

$$h_{j,j+1} := \begin{pmatrix} x_j - x_{j+1} - L_j c(\phi_{j+1} + \theta_{j+1}) \\ y_j - y_{j+1} - L_j s(\phi_{j+1} + \theta_{j+1}) \end{pmatrix} = 0 \tag{2.3}$$

where θ is the angle between the j-th WMR and $(j+1)$-th WMR described in Fig. 2.2 and $L_j > 0$ is the desired distance between the $j-$th WMRs. Following [1], we can then achieve the passive nonholonomic decomposition of the two WMRs

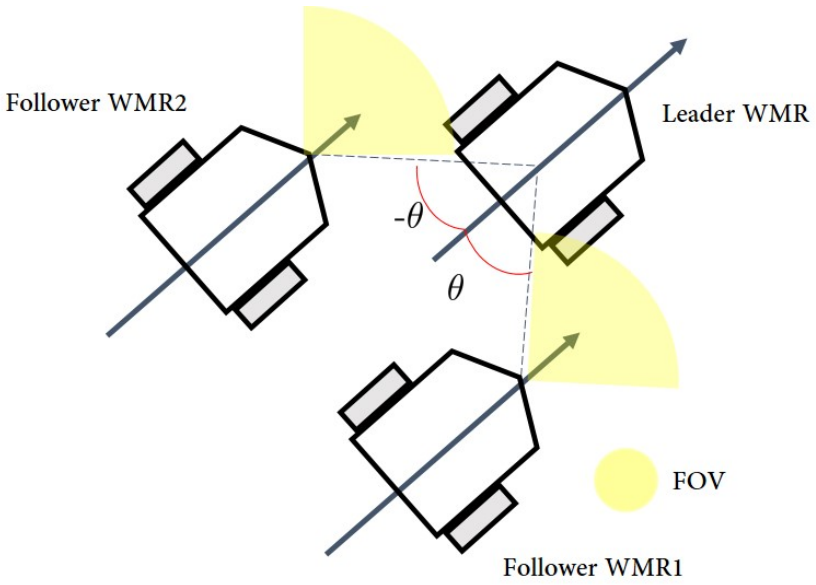

FIGURE 2.2: The θ of the follower WMRs

under the physical nonholonomic and virtual holonomic constraint 2.3 s.t.,

$$\dot{q}_{j,j+1} = \begin{bmatrix} (\mathcal{D}^{\top}_{j,j+1} \cap \Delta^{\top}_{j,j+1}) & \mathcal{D}^{c}_{j,j+1} \end{bmatrix} \begin{pmatrix} u_{L_{j,j+1}} \\ u_{C_{j,j+1}} \end{pmatrix} \tag{2.4}$$

where tangential distribution $\Delta^{\top}_{j,j+1}$ of $h_{j,j+1}$ is the null-space of the one form

$\frac{\partial h_{j,j+1}}{\partial q_{j,j+1}} \in \Re^{2\times 6}$ and normal distribution $\Delta^{\perp}_{j,j+1}(q_{j,j+1})$, the orthogonal complement of $\Delta^{\top}_{j,j+1}$ is w.r.t. $(\frac{\partial h_{j,j+1}}{\partial q_{j,j+1}})^T$ following [7]. We define

$$(\mathcal{D}^{\top}_{j,j+1} \cap \Delta^{\top}_{j,j+1}) = \begin{bmatrix} c\theta_j c\phi_j & 0 \\ c\theta_j s\phi_j & 0 \\ 0 & 1 \\ c(\phi_{j+1}+\theta-\phi_j)c\phi_{j+1} & 0 \\ c(\phi_{j+1}+\theta-\phi_j)s\phi_{j+1} & 0 \\ \frac{1}{L_j}s(\phi_j-\phi_{j+1}) & 0 \end{bmatrix} \in \Re^{6\times 2} \tag{2.5}$$

as the locked distribution (i.e., keeping the inter-WMR coordination shape $h_{j,j+1}$ locked); and

$\mathcal{D}^{c}_{j,j+1} = \mathcal{D}^{\top}_{j,j+1} \backslash (\mathcal{D}^{\top}_{j,j+1} \cap \Delta^{\top}_{j,j+1}) =$

$$\begin{bmatrix} c\phi_j & 0 \\ s\phi_j & 0 \\ 0 & 0 \\ -c(\phi_j-\phi_{j+1})c\phi_{j+1} & s(\phi_j-\phi_{j+1})c\phi_{j+1} \\ -c(\phi_j-\phi_{j+1})s\phi_{j+1} & s(\phi_j-\phi_{j+1})s\phi_{j+1} \\ -L_j s(\phi_{j+1}+\theta-\phi_j) & -L_j c(\phi_{j+1}+\theta-\phi_j) \end{bmatrix} \tag{2.6}$$

is the quotient distribution.

2.2 Attractive and Repulsive Potential Function

The system can move with satisfying nonholonomic constraint, however it is under restriction of two problems when the WMRs change their formation: 1) limitation of FoV range; 2) possibility of collision among WMRs. Here, we only consider the situation that WMRs change their formation from line to triangle and triangle to line. We redefine the estimated position [1] of the follower WMRs at the monocular camera, not the center of mass of each WMR, to make the most of the range of FoV.

First, we consider the limitation of FoV range. Even though, the system tries to keep the desired θ by $h_{j,j+1}$, the j-th WMR sometimes fails to see the pattern of the $j+1$-th WMR due to the mechanical defects and the trajectory that has sharp curve. For resolving this problem, we utilize the attractive potential field to keep the view of the camera put the pattern in. We define

$$\varphi_{f_{j,j+1}} := \begin{cases} \frac{1}{2}\eta(\alpha - A)^2 & (\alpha \geq A) \\ 0 & (\alpha < A) \end{cases}$$

where $\alpha = \angle p = tan\frac{p_y}{p_x}$ where $p = R^T(\theta)\begin{bmatrix} x^* - x \\ y^* - y \end{bmatrix}$ and A is attractive potential field. (x^*, y^*) is the position of following target, (x, y) is the estimated position

of j-th WMR. We can derive the equation s.t.,

$$\begin{aligned}\frac{d\varphi_{f_{j,j+1}}}{dt} &= \frac{\partial \varphi_{f_{j,j+1}}}{\partial q_{j,j+1}} \frac{dq_{j,j+1}}{dt} = \eta(a-A)\frac{\partial a}{\partial q_{j,j+1}}\frac{dq_{j,j+1}}{dt} \\ &= \eta(a-A)(\sec\frac{p_y}{p_x})^2 \frac{\frac{\partial p_y}{\partial q_{j,j+1}}p_x - p_y\frac{\partial p_x}{\partial q_{j,j+1}}}{p_x^2}\dot{q}_{j,j+1}\end{aligned}$$

, we then achieve

$$\begin{aligned}\frac{\partial p_x}{\partial q_{j,j+1}} &= \Big[0\ 0\ 0\ -c\theta\ -s\theta\ -s\theta(x^*-x)+c\theta(y^*-y)\Big] \\ \frac{\partial p_y}{\partial q_{j,j+1}} &= \Big[0\ 0\ 0\ s\theta\ -c\theta\ -c\theta(x^*-x)-s\theta(y^*-y)\Big]\end{aligned}$$

where $q_{j,j+1}$ is the configuration of the pair of the i-th and following target WMRs, and $\dot{q}_{j,j+1} = \mathcal{D}_{c_{j,j+1}} u_{C_{j,j+1}}$. We achieve

$$u_{C_{j,j+1}} = -\mathcal{D}^T_{c_{j,j+1}}(\frac{\partial \varphi_{f_{j,j+1}}}{\partial q_{j,j+1}})^T \tag{2.7}$$

, then $\frac{d\varphi_{f_{j,j+1}}}{dt} = -||\frac{\partial \varphi_{f_{j,j+1}}}{\partial q_{j,j+1}}\mathcal{D}_{c_{j,j+1}}||^2 \leq 0$.

Next, we consider the collision of WMRs. For this, we utilize repulsive potential function to avoid the collision. We define

$$\varphi_{c_{j,j+1}} := \begin{cases} \frac{1}{2}\eta(\frac{1}{d}-\frac{1}{D})^2 & (d<D) \\ 0 & (d\geq D)\end{cases}$$

where d is the distance between WMRs and D is desired potential field boundary. For collision avoidance, we use the center of each WMR, not the redefined estimated position, as the location of position (x', y') due to the physical shape of WMRs. This means $x' = x - \delta c\phi$ and $y' = y - \delta s\phi$ where δ is the distance between the camera and the center of WMR. We can then achieve $d = \sqrt{\frac{(x'-x^*)^2}{a^2} + \frac{(y'-y^*)^2}{b^2}}$ where (x', y') is the position of i-th WMR, (x^*, y^*) is j-th WMR, a and b are each major axis and minor axis of the ellipse for the potential field. The reason why the shape of the potential field is ellipse is because of the physical size of the WMRs as you can see in Fig. 2.1, the distance to move and the trajectory while changing the formation. We can also change the form of the potential field with matching the shape, size of the each WMR and the formation WMRs have to make. Now, we can derive the equation s.t.,

$$\frac{d\varphi_{c_{j,j+1}}}{dt} = \frac{\partial \varphi_{c_{j,j+1}}}{\partial q_{j,j+1}} \frac{dq_{j,j+1}}{dt} = -\eta(\frac{1}{d} - \frac{1}{D})\frac{1}{d^2}\frac{\partial d}{\partial q}\frac{dq_{j,j+1}}{dt} = -\eta(\frac{1}{d} - \frac{1}{D})\frac{1}{d^3}$$

$$\cdot \left[0 \;\; 0 \;\; 0 \;\; \frac{x'-x^*}{a^2} \;\; \frac{y'-y^*}{b^2} \;\; \frac{(x'-x^*)\delta s\phi}{a^2} + \frac{-(y'-y^*)\delta c\phi}{b^2}\right] \dot{q}_{j,j+1}$$

where q is the configuration of the pair of the i-th and following target WMRs, and $\dot{q}_{j,j+1} = \mathcal{D}_{c_{j,j+1}} u_{C_{j,j+1}}$. We achieve

$$u_{C_{j,j+1}} = -\mathcal{D}^T_{c_{j,j+1}} (\frac{\partial \varphi_{c_{j,j+1}}}{\partial q_{j,j+1}})^T \tag{2.8}$$

, then $\frac{d\varphi_{c_{j,j+1}}}{dt} = -||\frac{\partial \varphi_{c_{j,j+1}}}{\partial q_{j,j+1}} \mathcal{D}_{c_{j,j+1}}||^2 \leq 0$.

2.3 Control Design

By using the control $u_{c_{j,j+1}}$, we can then regulate the inter-WMR coordination. For this, we design $u_{c_{j,j+1}}$ s.t.,

$$u_{C_{j,j+1}} = -\mathcal{D}_{j,j+1}^{cT}(q_{j,j+1}) \cdot \left[\frac{\partial h_{j,j+1}}{\partial q_{j,j+1}}\right]^T \left[\frac{\partial \varphi_{h_{j,j+1}}}{\partial h_{j,j+1}}\right]^T \in \Re^2 \tag{2.9}$$

where $\varphi_{h_{j,j+1}}(h_{j,j+1}) \geq 0$ is a suitably defined positive-definite potential function to enforce $h_{j,j+1} = 0$. We then, have

$$\begin{aligned} \frac{d\varphi_{h_{j,j+1}}}{dt} &= \frac{\partial \varphi_{h_{j,j+1}}}{\partial h_{j,j+1}} \frac{\partial h_{j,j+1}}{\partial q_{j,j+1}} \dot{q}_{j,j+1} \\ &= \frac{\partial \varphi_{h_{j,j+1}}}{\partial h_{j,j+1}} \frac{\partial h_{j,j+1}}{\partial q_{j,j+1}} \mathcal{D}_{c_{j,j+1}} u_{C_{j,j+1}} \\ &= -||u_{C_{j,j+1}}||^2 \leq 0 \end{aligned} \tag{2.10}$$

becuase $\frac{\partial h_{j,j+1}}{\partial q_{j,j+1}} \cdot [\mathcal{D}_{j,j+1}^{\top} \cap \Delta_{j,j+1}^{\top}] \cdot u_{L_{j,j+1}} = 0$ is trivial from 2.4. This means $\varphi_{h_{j,j+1}}(t) \leq \varphi_{h_{j,j+1}}(0)$, that is, $\varphi_{h_{j,j+1}}$ will be decreasing if $u_{c_{j,j+1}} \neq 0$. If we define $\varphi_{j,j+1} := \varphi_{h_{j,j+1}} + \varphi_{c_{j,j+1}} + \varphi_{f_{j,j+1}}$, we can draw a conclusion that φ will be decreasing from combining 2.7 - 2.10:

$$u_{C_{j,j+1}} = -\mathcal{D}_{c_{j,j+1}}^{T} \frac{\partial \varphi_{j,j+1}}{\partial q_{j,j+1}}^T \tag{2.11}$$

It means $\varphi_{j,j+1}(t) \leq \varphi_{j,j+1}(0)$, that is $\varphi_{j,j+1}$ will be decreasing if $u_{c_{j,j+1}} \neq 0$.

Now, suppose that the velocity command (v_j, w_j) of the j-th WMR is given

(e.g., the forward and angular velocities of the leader WMR will be directly tele-controlled by a remote user). Then, from 2.4, we can compute the forward and angular velocity commands of the $(j+1)$-th WMR as

$$
\begin{aligned}
v_{j+1} &= u^1_{L_{j,j+1}} c(\phi_{j+1} + \theta - \phi_j) \\
&- \begin{bmatrix} c(\phi_j - \phi_{j+1}) & -s(\phi_j - \phi_{j+1}) \end{bmatrix} u_{c_{j,j+1}} \\
w_{j+1} &= \frac{1}{L_j} u^1_{L_{j,j+1}} s(\phi_j - \phi_{j,j+1}) \\
&- L_j \begin{bmatrix} s(\phi_{j+1} + \theta - \phi_j) & c(\phi_{j+1} + \theta - \phi_j) \end{bmatrix} u_{c_{j,j+1}}
\end{aligned}
$$

, repeating it, we can achieve the velocity control input (v_j, w_j) for all the WMR, $j = 1, ..., n$. Here, note that if $\phi_j - \phi_{j+1} = \frac{\pi}{2}, w_{j+1} = \frac{v_j}{L}$ with $v_{j+1} = 0$, it can cause the singularity of the system because , $j+1$-th WMR has to rotate instantaneously to keep its heading to the center of the $j - th$ WMR and it is impossible behavior with the limited sensing range.

2.4 Simulation

The simulation to verify the proposed algorithm is preperfomed before the experiment with the real robots. It consists of 5 different formations with 39 tanks (for better visualization, securing the association between this thesis and military operation) and the resulst are captured in Fig. 2.3 - 2.7. The explanation of the simulation results in terms of the reason for choosing the formations is shortened

because of the military security. The mathmatical experession for them is related to 2.3.

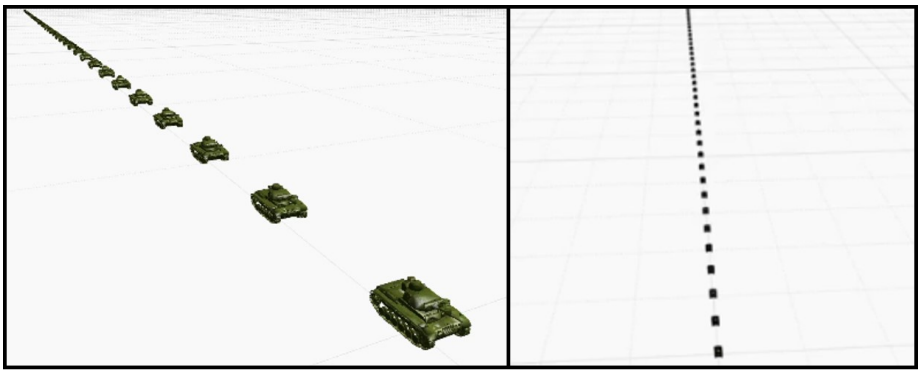

FIGURE 2.3: Simulation result of the 39 tanks making various shape of the formation under the distributed control : Formation #1

First, we make the tanks drive in line shape formation. It is already shown and demonstrated with 29 WMRs in the previous study [1], but we simulate it agiain becuase the line graph topology is also important in this thesis. The WMRs have to move in linear formation while passing the narrow space in the experiment implemented with the teleoperation. In military, especially in an armor troop, tanks have to move like n-trailer system to pass the narrow terrain or in the usual peacetime. We exclude the θ_{j+1} in the consideration components such as,

$$h_{j,j+1} := \begin{pmatrix} x_j - x_{j+1} - L_j c\phi_{j+1} \\ y_j - y_{j+1} - L_j s\phi_{j+1} \end{pmatrix} = 0$$

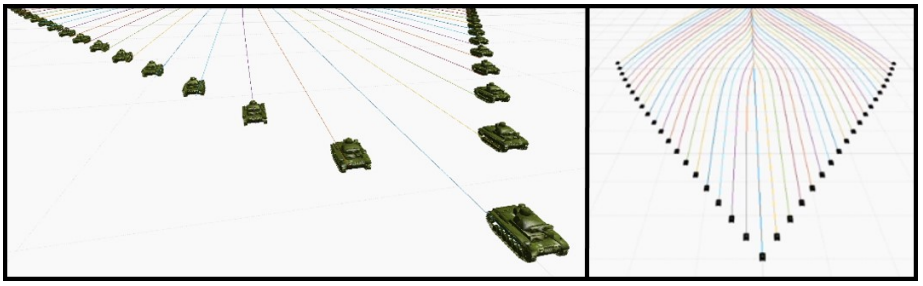

FIGURE 2.4: Simulation result of the 39 tanks making various shape of the formation under the distributed control : Formation #2

Next, the tanks are maneuvering in triangle shape formation. It is also important becuase of the same reason with first one. In military, a platoon of the tanks make the triangular graph topology in a wide area. The tanks sometimes have to make inverse-trianlge shape formation in according to the tactical doctrine, in this thesis, we only consider triangle shape formation. It can be achieved to set θ_{j+1} as the commander wants to. Note that, the value of θ for the robots in the left side, of course, have opposite sign with the right side. Even though it is simulation, we set the value of θ not to overrun the FoV range of the sensor (monocular camera) used in real experiment for securing the plausibility. It is also possible to achieve it with setting the attractive potential field properly even with the value of θ bigger than the FoV range, but it shows different behavior in the process of making the formation shape and spends more time for making the desired formation becuase of the insufficient DoF (degree of freedom) of the tanks.

From here, the results are confined to the simulation becuase of the short of the number of WMRs. However, we show the simulation results with the new algorithm, it is easy to make it operate with real WMRs in near future.

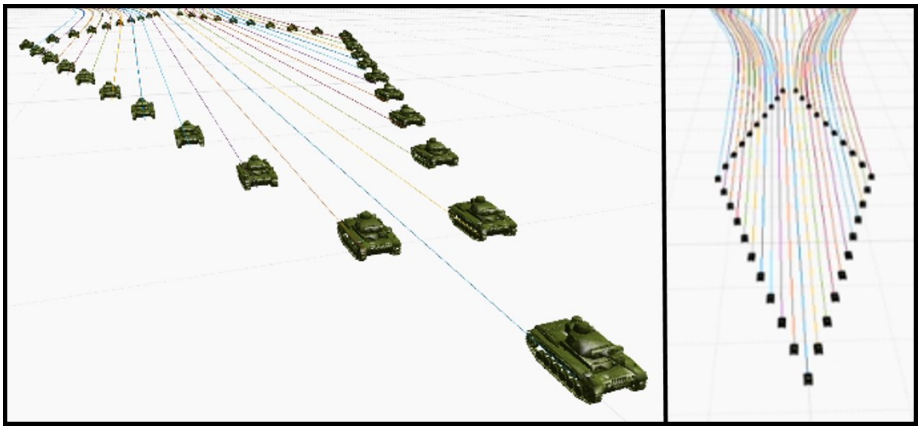

FIGURE 2.5: Simulation result of the 39 tanks making various shape of the formation under the distributed control : Formation #3

The tanks are moving in diamond shape formation. In these days, various type of robots are used in the important military events for the performance. The diamond shape has the symbolic meaning of a strong will for protecting the country in Korean military and the second lieutenant, the very first rank in terms of officers. have silver rank insignia with a diamond. It can be applied to the robots mobilized in the commission ceremony to celebrate new officers. We can achieve this formation with switching the sign of θ of each WMR from the 12-th line up to the final line.

There are no specific reason for making the formation in the next two simulation results, but they have enough meaning for verifying the new algorithm to apply to various and complex shapes that are not common like the line, triangle and diamond shape.

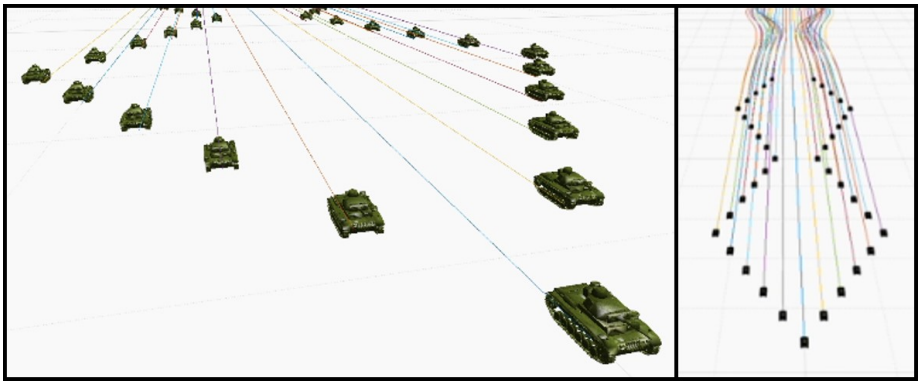

FIGURE 2.6: Simulation result of the 39 tanks making various shape of the formation under the distributed control : Formation #4

We give the same value for θ of 2-6-th line, 12-16-th and switch the sign for 7-11-th line, 17-20-th.

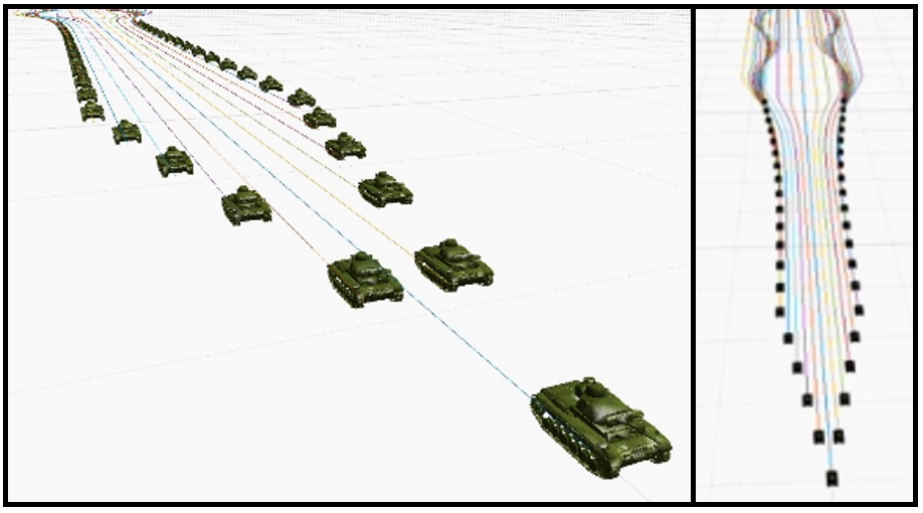

FIGURE 2.7: Simulation result of the 39 tanks making various shape of the formation under the distributed control : Formation #5

We set the θ of the WMRs from 7-th line as zero.

Chapter 3

Estimation and Predictive Display

3.1 Distributed Pose Estimation

3.1.1 EKF Pose Estimation of Leader WMR

All the WMRs run the EKF algorithm for fusing their IMU to get the (relative) measurement and estimate the pose of each WMR in a distributed manner. Following [1], the leader WMR is supposed to function with the SLAM algorithm of [19] by using the LiDAR sensor, and we fuse this information with the IMU. For this, we utilize the technique of error-state EKF.

Let us start with defining the state of this IMU-LiDAR sensor fusion s.t.,

$$\chi_1 := \Big[p_1; \quad \xi_1; \quad \phi_1; \quad b_{a_1}; \quad b_{g_1}\Big] \in \Re^8 \tag{3.1}$$

where $p_1 := [x_1; y_1] \in \Re^2, \xi_1 := [\dot{x}_1; \dot{y}_1] \in \Re^2$, and $b_{a_1} = [b_{a_1,x}; b_{a_1,y}] \in \Re^2$ and $b_{g_1} \in \Re$ are the biases of the accelerometer and gyroscope of the IMU.

Then, the linearized continuous-time error state equation can be obtained by

$$\dot{\tilde{\chi}}_1 = F_1(t)\tilde{\chi}_1 + G_1(t)n_1 \tag{3.2}$$

where $\tilde{(\hat{})} = (\dot{}) - \hat{(\hat{})}$ is the difference between the true state and the estimated state. This continuous-time equation can then be discretized at time t_k, and we can obtain the error state covariance propagation equation s.t.,

$$\begin{aligned} P^{\chi_1}_{k+1|k} \simeq (I_8 + F_{1,k}dt)P^{\chi_1}_{k|k}(I_8 + F_{1,k}dt)^T \\ + (G_{1,k}dt)Q_1(G^T_{1,k}dt) \end{aligned}$$

where $P^{\chi_1}_{k|k}, P^{\chi_1}_{k+1|k}$ are the priori, posteriori covariance of the leader WMR at k, respectively.

As a measurement for EKF, we use the pose measurement obtained by the LiDAR-SLAM, i.e.,

$$z_{\text{SLAM}} = \begin{pmatrix} p_1 \\ \phi_1 \end{pmatrix} + \begin{pmatrix} n_{p_1} \\ n_{\phi_1} \end{pmatrix}$$

To correct the error state $\tilde{\chi_1}$ with measurement received at $k+1$, the Kalman gain is computed s.t.,

$$\begin{aligned} S_{k+1} &= H_1 P^{\chi_1}_{k+1|k} H_1^T + R_1 \\ K_{k+1} &= P^{\chi_1}_{k+1|k} H_1^T S^{-1}_{k+1} \end{aligned} \tag{3.3}$$

Using this Kalman gain, the propagated error state and its covariance are updated through the standard EKF algorithm s.t.,

$$\begin{aligned} \hat{\chi}_{1,k+1|k+1} &= \hat{\chi}_{1,k+1|k} + K_{k+1} \tilde{z}_{\text{SLAM},k+1} \\ P^{\chi_1}_{k+1|k+1} &= P^{\chi_1}_{k+1|k} - P^{\chi_1}_{k+1|k} H_1^T S^{-1}_{k+1} H_1 P^{\chi_1}_{k+1|k} \end{aligned} \tag{3.4}$$

3.1.2 EKF Pose Estimation of Follower WMRs

The propagation step of the "simple" follower WMRs is similar to that of the leader WMR. The only difference is using the measurement from the camera,

which is given by

$$z_{j,\text{camera}} = \begin{pmatrix} z_p \\ z_\phi \end{pmatrix} + \begin{pmatrix} n_{p_j} \\ n_{\phi_j} \end{pmatrix}$$

where $z_p := R_{\mathcal{O}}^{\mathcal{G}_j}(\phi_j)\ (p_{j-1} - p_j) \in \Re^2$ and $z_\phi := (\phi_{j-1} - \phi_j) \in \Re$ are the relative position and bearing between the $(j-1)$ and the j-th WMR expressed in the j-th WMR's frame.

Then, when the measurement is received, we can update the state and covariance of the error state of the j-th WMR similar to 3.3 and 3.4.

3.2 Predictive Display for Distributed WMRs Teleoperation

This section shows the interface for the teleoperation of the distributed nonholonomic WMRs. The key enabling component for this is the predictive display, which aloows us to address the two peculiar issues of the distributed robotics on the problem of teleoperation, namely, 1) inherenct uncertainty of the human perception stemming from the limitation of the onboard sensing (e.g., accumulation of uncertainty from the leader to the last WMRs with onboard relative measurement) and the transmission delay through the multi-hop peer-to-peer communication; and 2) complexity of the kinematics, and subsequently difficulty of tele-controlling the motion, of the platoon of large number of distributed robots,

which, even if reduced to a (more familiar) n-trailer system in this thesis, is still very difficult to tele-control for most users particularly in an obstacle-cluttered environment.

To circumvent these two issues of distributed robotics for teleoperation, we design the predictive display to be composed of the two stages: 1) estimation propagation stage, where the (uncertain) pose estimate of each WMR, received at the current time t with the transmission delay, is probabilistically propagated so that we can estimate its pose at t with associated uncertainty; and 2) prediction propagation stage, where the pose of each WMR at t, as obtained via the estimation propagation, is forward-propagated with the current user command so that we can predict the course of the platoon motion over the prediction time horizon. We also adopt unscented transformation, since it allows us to propagate random variable via a nonlinear map.

We then present this predictive display information (i.e., estimated pose and predicted pose) to the user by overlaying them on the LiDAR-SLAM map with their position and orientation uncertainties respectivlely rendered by the enlarged shape and the heading angle cone of each WMR, with their center location/angle and the sweeping/size/angle determined by the corresponding mean and covariance.

By seeing this predictive display, the human user is then able to predict the procession of the distributed n-WMRs in the environment with obstacles, examine the likelihood and location of collisions, and adjust their teleoperation command.

This predictive display turns out to be crucial for the teleoperation of the distributed nonholonomic WMRs, since, if it were not for, it is fairly difficult for human users to predict and control the complex motion and internal articulation of the group of the distributed nonholonomic WMRs, even if their number is only three.

The derivation of predictive display may also be extended to determine, e.g., the maximum possible number of distributed robots to safety navigate among obstacles, given the robot sizes, inter-obstacle distances, transmission delay of the peer-to-peer communication and onboard sensor accuracy. The idea of predictive display may also be expanded for the general problem of "teleoperation with uncertainty", by indicating the best possible control direction given the sensor uncertainty, parameter estimation error, actuation inaccuracy, etc. These are the topics of future research. The information of communication architecture for control, estimation and predictive display is shown in Fig. 3.1

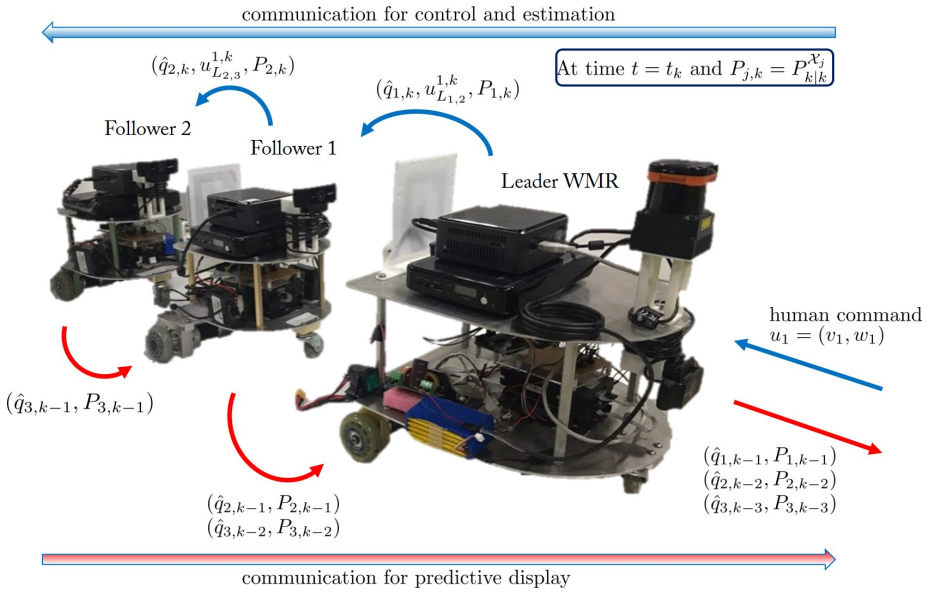

FIGURE 3.1: Communication architecture among the WMRs and the flowing information

Chapter 4

Experiment

4.1 Test Setup

We use three nonholonomic WMRs shown in Fig. 1. All WMRs have one passive caster in front of each WMR to prevent tipping-over and two rear differential-drive wheels driven by Maxon® BLDC motors under velocity control mode. Arduino Uno MCU (micro-controller unit) delivers the command from Intel® NUC7i7. The leader WMR has a LiDAR (Hokuyo UTM-30LX-EW) and an iMU sensor (MPU-9250, only (x, y)-accelerometer and yaw gyroscope used) to estimate its pose and hold the information of the driving environment. Monocular web-cam (Logitech C922, 640 $\times$ 480) is used for FPV. The follower WMRs have a front view monocular web-cam (Logitech C922, 1280 $\times$ 720) and the same

IMU sensor as the leader. Known patterns similar to Olson [20] are also attached at all of each WMR for using information from monocular camera brought by OpenCV for pattern recognition as the measurement of the estimator. We use the larger size of patterns campared to [1] and maximize the resolution of the camera to secure a clear view of the patterns for providing better condition while chaing the formation. The materials that are not shown in 1.1 but used in the test is figured in Fig. 4.1, 4.2.

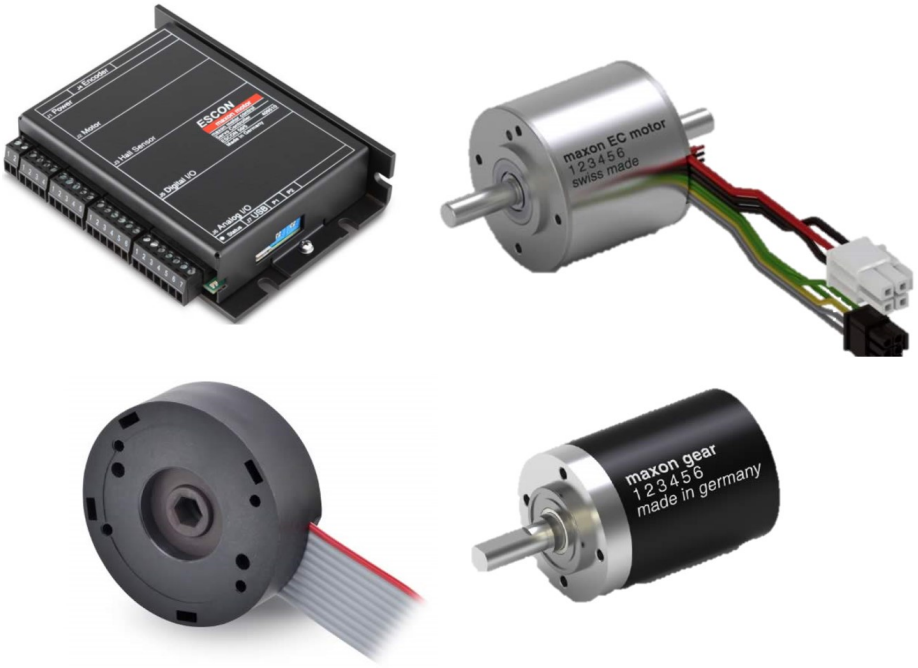

FIGURE 4.1: The driver, motor, gear, encoder set made by Maxon® used in the test

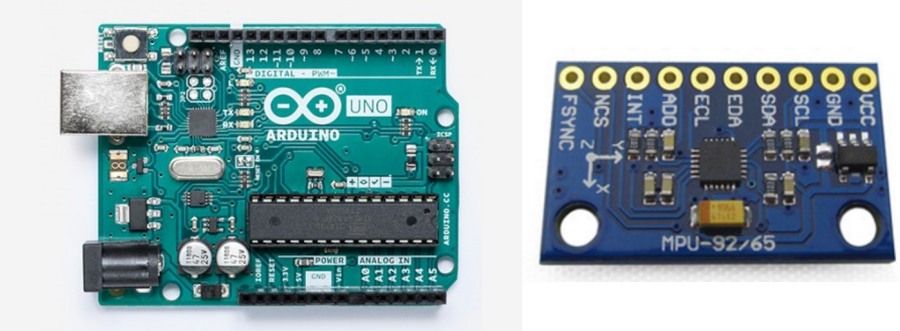

FIGURE 4.2: MPU-9250 (IMU sensor for getting the information of acceleration and yaw angular velocity) and Arduino Uno for sending the information from the IMU to computer (NUC7i7) and the velocity input to the motor set

Computing OS of all WMRs is Robot Operating system (ROS). RVIZ (3D visualization tool of ROS) is utilized to render the map described by LiDAR-SLAM. We also render the current and future pose estimates of the WMRs. The rendered feature is visualized by the leader and the master PC bring it for the user. We use UDP protocol to implement peer-to-peer communication among WMRs and with the user interface. We use the Omega3 haptic device as the commanding device and the wireless keyboard connected with the NUC7i7 of the leader WMR to deliver the command for the formation reconfiguration. Other base setup information is stated in [1].

4.2 Demonstrate the Proposed Algorithm

Before the experiment for implementation of the scenario, we conduct the experiment for demonstrating the new algorithm. The three WMRs as shown in Fig. 1 are used. First, we operate the WMRs without attractive force. Second, we operate the WMRs without repulsive force. Third, we operate the WMRs with the new algorithm. We order the WMR change their formation from line graph topology to triangular graph topology for all performed experiment. The experiment results are captured in Fig. 4.3 - 4.5.

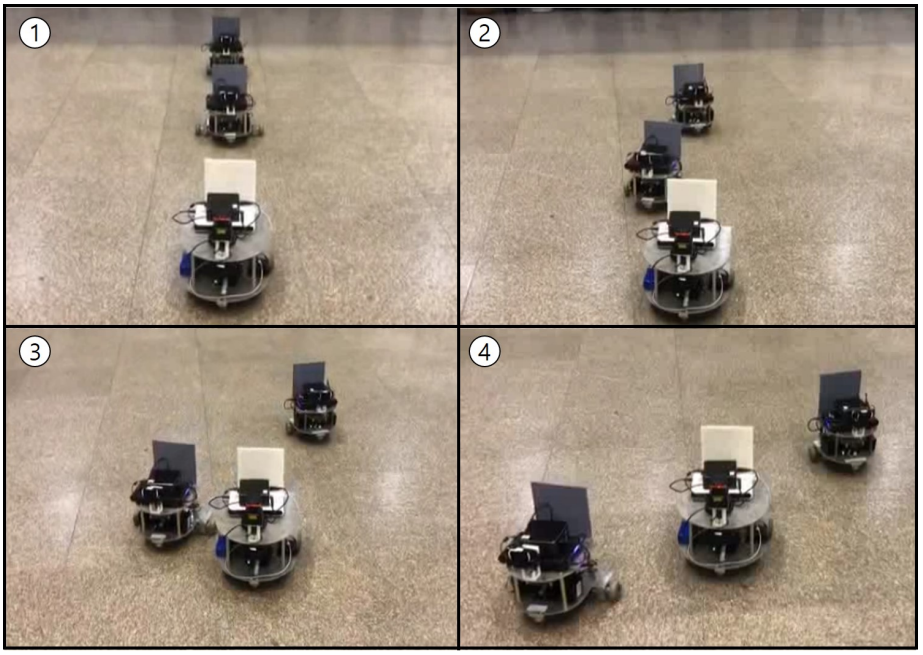

FIGURE 4.3: The system failure because of the absence of the attractive force to keep the θ

We can see the follower WMRs miss the pattern of the leader WMR, as a result, the follower WMRs fail to estimate their present pose and it leads to the system collapse.

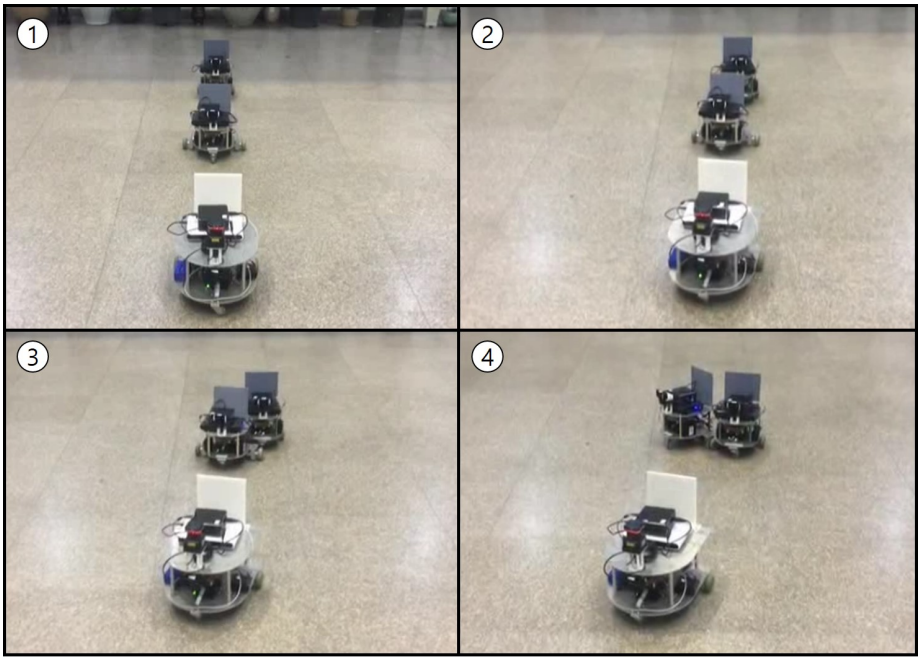

FIGURE 4.4: The system failure because of the absence of the repulsive force to prevent the collision among the WMRs

The follower WMRs collide each other, as a result, the user has to stop operating the system.

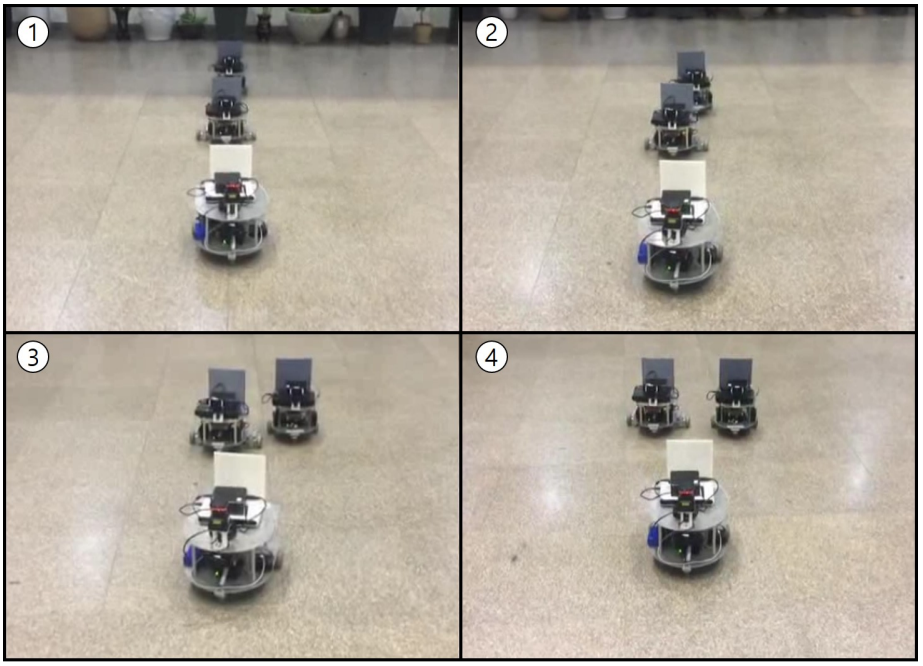

FIGURE 4.5: Verify, Demonstate the neccessity of the proposed algorithm (attractive and repulsive potential field)

It shows the WMRs make the triangular shape formation successfully.

We demonstrate the feasibility of the proposed algorithm from Fig. 4.3 - 4.5. We can then trust the algorithm and apply it for the experiment in unknown driving environment.

4.3 Teleoperation Experiment with the Algorithm

Next, we conduct teleoperation experiment with the new algorithm at the real building lounge. The environment is shown in Fig. 4.6. The task goal is to change their formation suitably in according to the situation of the driving environment. For this, a human user tele-drives the WMRs starting from the red point, move along the blue dotted line without collision with the several obstacles and the wall of the narrow space and switch the formation at the yellow area in Fig. 4.6.

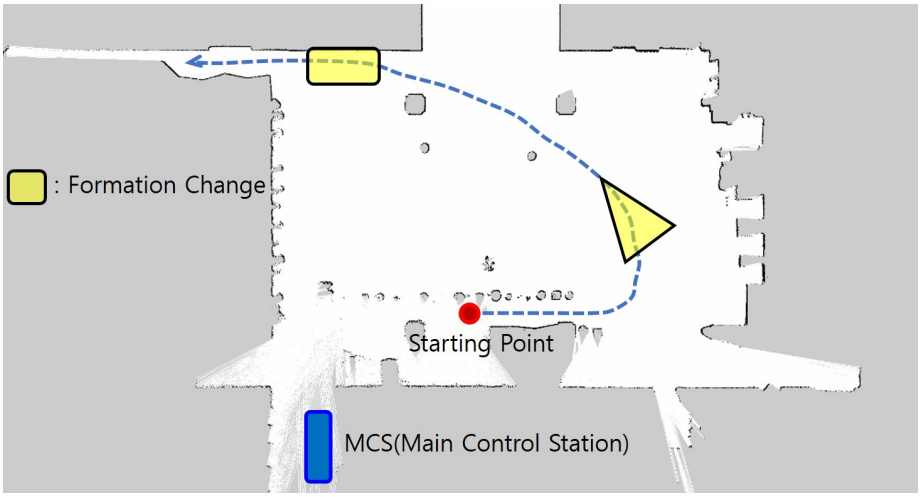

FIGURE 4.6: The environment map made by LiDAR-SLAM for the experiment: blue box indicate the MCS (main control station); blue dotted line is the trajectory that WMRs have to track; yellow boxes are the area of formation reconfiguration

The user can't see the WMRs directly, so the user have to rely on the information of predictive display and FPV. The master interface consists of one monitor, one

haptic device and one wireless keyboard as depicted in Fig. 4.7.

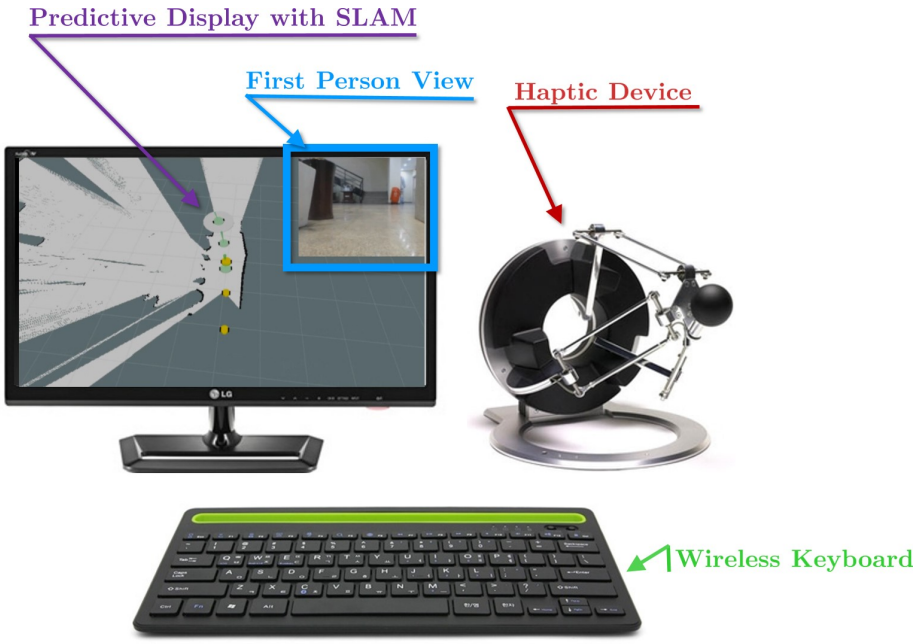

FIGURE 4.7: User interface in the MCS. Omega3 is used for haptic device, the monitor shows predictive display with SLAM and FPV

The monitor displays the FPV camera view and the LiDAR-SLAM map. The haptic device is used only as a pointing device with haptic feedback turned off. The predictive display shows the current pose and future pose estimates of all the WMRs. The yellow colored objects refers to the present pose, green colored objects refers to the future pose which is the WMRs are moving with the present speed and the present direction for 20 seconds. The gray colored circle refers to the information of the possibility of the collision with the surroundings. The

orientation of the predictive display and LiDAR-SLAM map are rotated with FPV camera view to avoid the user confusion.

The results of the experiment with the distributed nonholonomic WMRs: one leader and two followers, all with peer-to-peer communication are shown in Fig. 4.8 - 4.12. Fig. 4.9, 4.11 are the process of formation reconfiguration.

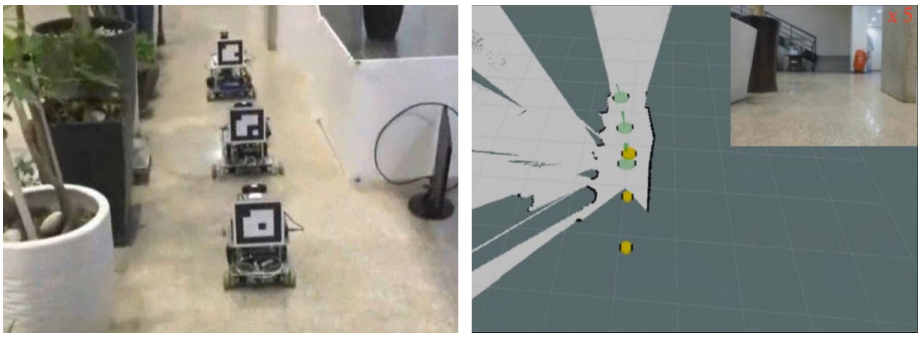

FIGURE 4.8: Formation reconfiguration experiment in real environment, phase #1 : Linear formation

The WMRs are moving in line shape formation to pass the narrow space from the starting point. We set the desired distance between j-th and $j+1$-th WMR, L, as $1.2m$ and the desired angle, θ, 0.

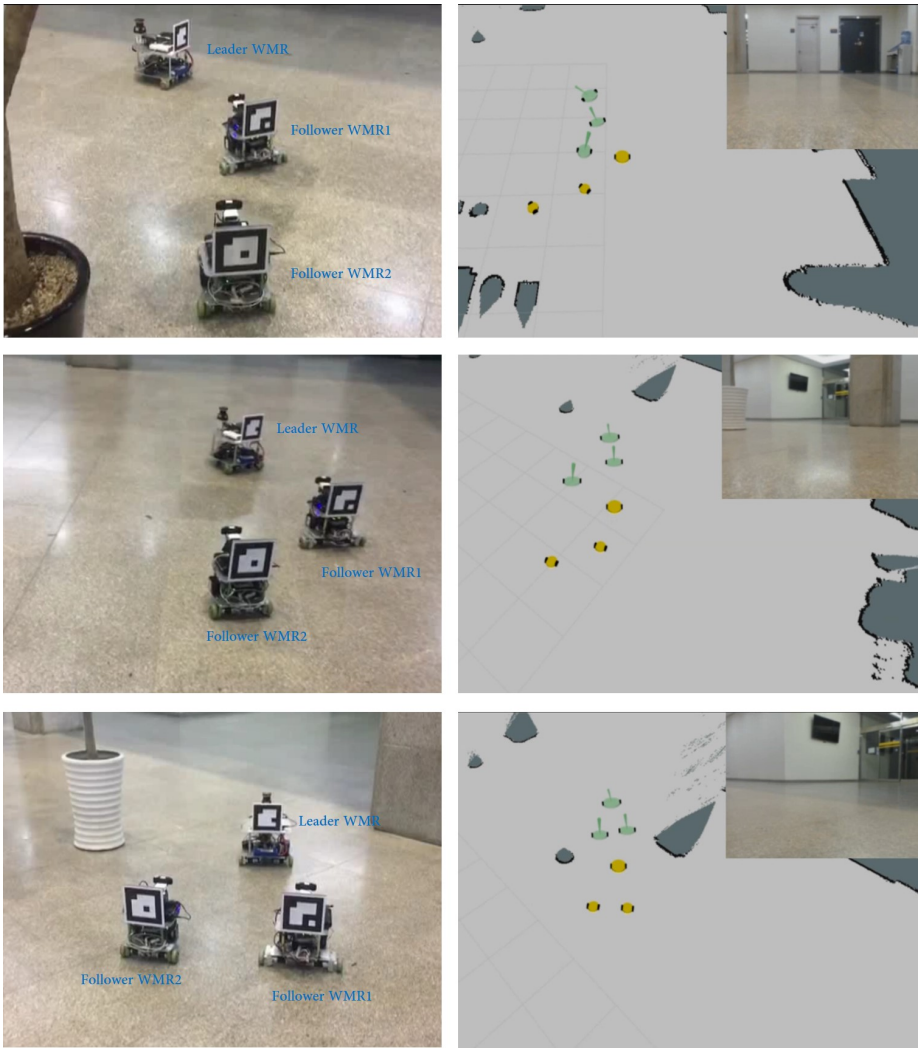

FIGURE 4.9: Formation reconfiguration for making triangle shape

The WMRs change their formation from line graph topology to triangular graph topology without any collision while not running off the FoV of the follower

WMRs. Here, $L_{1,2}$, $L_{1,3}$ are also $1.2m$ and $\theta_{1,2}$ is $-32°(0.559rad)$ and $\theta_{1,3}$ is $32°$. The attractive repulsive field is set to $35°(0.611rad)$ because the FoV of used webcam is $74°(\pm 37°)$.

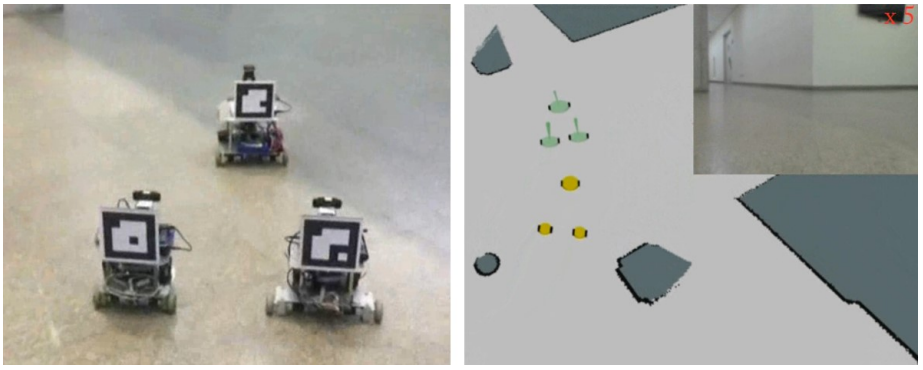

FIGURE 4.10: Formation reconfiguration experiment in real environment, phase #2 : triangular formation

The WMRs are moving in triangle shape formation in the open area. As we mentioned before in Sec. 2, it is impossible to make the inverse triangular formation. If the leader WMR is located in the very rear position, follower WMRs are unable to estimate their pose due to the limited sensing of the monocular cameras. We remain resolving this problem for future works.

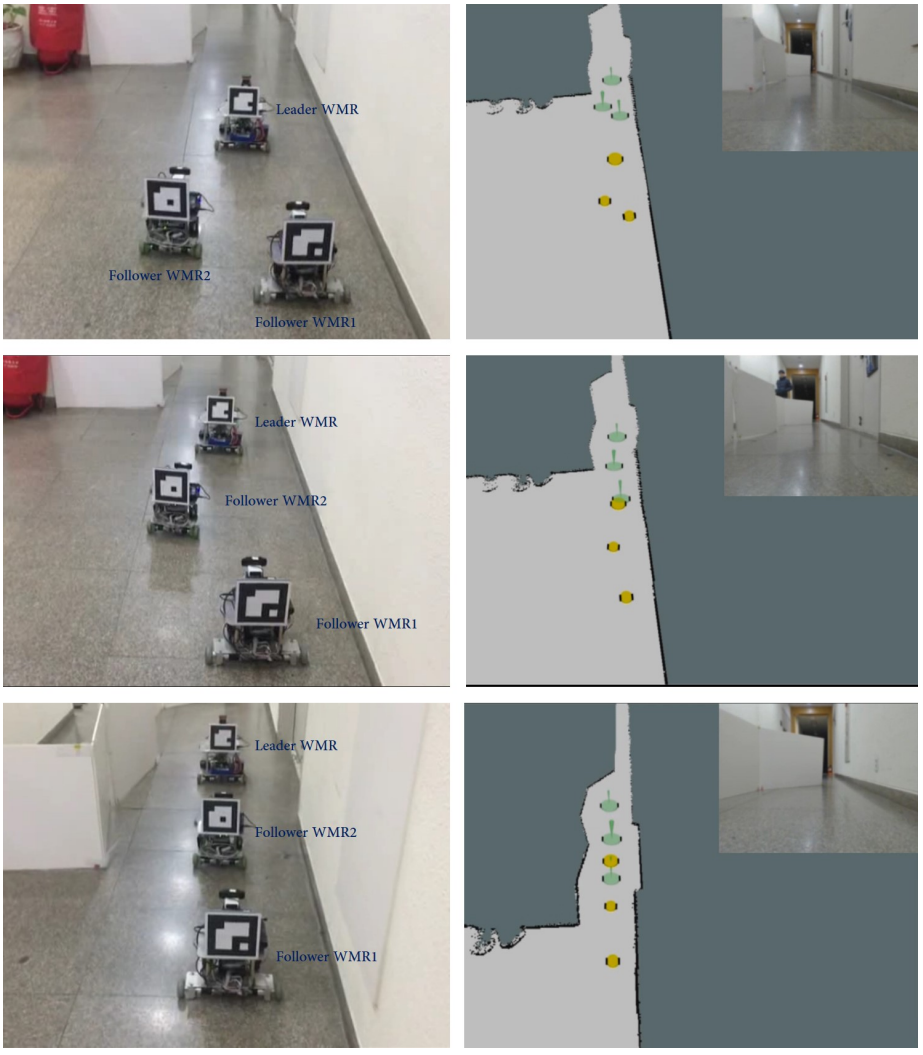

FIGURE 4.11: Formation reconfiguration for making line shape

The WMRs are making line shape formation again while switching the order of the follower WMRs compared to the strarting formation. The parameters of 2.3

are same as the first line shape formation and the ID of the pattrern the follower WMRs have to see is changed.

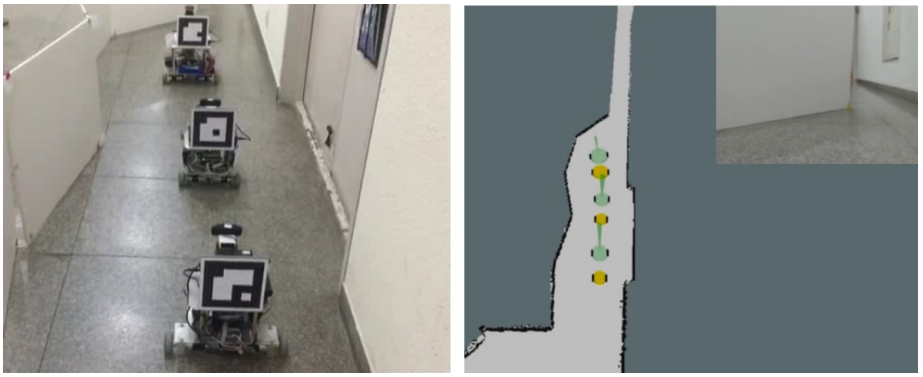

FIGURE 4.12: Formation reconfiguration experiment in real environment, phase #3 : Linear formation

The WMRs maneuver in line shape formation because the FPV camera shows the front narrow terrain to the user and arrive at the goal.

From the figures, we can see that: 1) formation reconfiguration is successful even with the changing driving environment; 2) teleoperation with FPV and the predictive display in the SLAM map is efficient in unknown space where the fully autonomous system is hard to work.

Chapter 5

Conclusion

To try to teleoperate a group of distributed robots, the following issues are faced with: 1) how to design the control under distribution constraint, while maintaining a certain desired formation regardless of arbitrary human command; 2) how to make the envirionment for the user for teleoperating the system intuitively and efficiently, even in the driving environment with obstacles and the pose information of each robot is has high unceratinty becuase of distribution constraint. The previous study [1] shows the framework to resolving the issues mentioned above. Whenever one attempts to change the formation of a group of the robots, they also encounter with the following issues: 1) how to overcome the limitation of the sensing range; 2) how to prevent collision among the robots. This thesis proposes a novel framework. It stands upon passive nonholonomic decomposition, which allows us to split the platoon kinematics into the inter-WMR coordination and

collective motion aspects. To switch formation effectively, a novel control design combined with the new algorithm is proposed, which provides the wide utility of the system. Simulation and experiment are also performed and exhibit the effectiveness of the proposed formation reconfiguration framework.

Some possible future work topics are: 1) implementation of various formation shape with more WMRs; 2) finding or developing other method for sensing for follower WMRs to unthread from limitation of FoV.

Bibliography

[1] C. Ha, J. Yoon, C. Kim, Y. Lee, S. Kwon, and D. Lee. Teleoperation of a platoon of distributed wheeled mobile robots with predictive display. *Autonomous Robots*, 42(2):1819–1836, 2018.

[2] J. P. Desai, J. Ostrowski, and V. Kumar. Controlling formations of multiple mobile robots. In *Robotics and Automation, 1998. Proceedings. 1998 IEEE International Conference on*, volume 4, pages 2864–2869. IEEE, 1998.

[3] R. M. Murray and S. S. Sastry. Nonholonomic motion planning: Steering using sinusoids. *IEEE Transactions on Automatic Control*, 38(5):700–716, 1993.

[4] R. Wei and R. Beard. Distributed consensus in multi-vehicle cooperative control theory and applications. *London: Springer-Verlag*, pages 1949–3053, 2008.

[5] D. Lee and P. Y. Li. Passive decomposition approach to formation and maneuver control of multiple rigid bodies. *Journal of Dynamic Systems, Measurement, and Control*, 129(5):662–677, 2007.

[6] D. Lee. Passive decomposition and control of nonholonomic mechanical systems. *IEEE Transactions on Robotics*, 26(6):978–992, 2010.

[7] D. Lee and P. Y. Li. Passive decomposition of mechanical systems with coordination requirement. *IEEE Transactions on Automatic Control*, 58(1): 230–235, 2013.

[8] D. Lee and K. Y. Lui. Passive configuration decomposition and passivity-based control of nonholonomic mechanical systems. *IEEE Transactions on Robotics*, 33(2):281–297, 2017.

[9] O. Khatib. Real-time obstacle avoidance for manipulators and mobile robots. In *Autonomous robot vehicles*, pages 396–404. Springer, 1986.

[10] Y. Koren and J. Borenstein. Potential field methods and their inherent limitations for mobile robot navigation. In *Robotics and Automation, 1991. Proceedings., 1991 IEEE International Conference on*, pages 1398–1404. IEEE, 1991.

[11] J. Kim and P. K. Khosla. Real-time obstacle avoidance using harmonic potential functions. *IEEE Transactions on Robotics and Automation*, 8(3): 338–349, 1992.

[12] S. S. Ge and Y. J. Cu. Dynamic motion planning for mobile robots using potential field method. *Autonomous robots*, 13(3):207–222, 2002.

[13] J. P. Desai, J. Ostrowski, P. James, and V. Kumar. Modeling and control of formations of nonholonomic mobile robots. *IEEE transactions on Robotics and Automation*, 17(6):905–908, 2001.

[14] D. Lee, A. Franchi, H. Son, C. Ha, H. H. Bülthoff, and R. P. Giordano. Semiautonomous haptic teleoperation control architecture of multiple unmanned aerial vehicles. *IEEE/ASME Transactions on Mechatronics*, 18(4): 1334–1345, 2013.

[15] A. Franchi, C. Secchi, H. Son, H. Bülthoff, and R. P. Giordano. Bilateral teleoperation of groups of mobile robots with time-varying topology. *IEEE Transactions on Robotics*, 28(5):1019–1033, 2012.

[16] E. J. Rodríguez-Seda, J. J. Troy, C. A. Erignac, A. Charles, P. Murray, D. M. Stipanovic, and M. W. Spong. Bilateral teleoperation of multiple mobile agents: Coordinated motion and collision avoidance. *IEEE Transactions on Control Systems Technology*, 18(4):984–992, 2010.

[17] T. Balchr and R. C. Arkin. Behavior-based formation control for multirobot teams. *IEEE transactions on robotics and automation*, 14(6):926–939, 1998.

[18] J. Chen, D. Sun, J. Yang, and H. Chen. Leader-follower formation control of multiple non-holonomic mobile robots incorporating a receding-horizon

scheme. *The International Journal of Robotics Research*, 29(6):727–747, 2010.

[19] G. Grisetti, C. Stachniss, and W. Burgard. Improved techniques for grid mapping with rao-blackwellized particle filters. *IEEE transactions on Robotics*, 23(1):34–46, 2007.

[20] Edwin Olson. Apriltag: A robust and flexible visual fiducial system. In *Robotics and Automation (ICRA), 2011 IEEE International Conference on*, pages 3400–3407. IEEE, 2011.

요약

본 논문에서는 변화하는 주행 환경에서 분산 제약 하에 다수의 원격으로 제어되는 논홀로노믹 이동형 로봇 대형 재구성 제어에 대한 새로운 프레임워크를 제시하였다. 센싱과 컴퓨팅 능력이 갖추어진 온보드 시스템 로봇들을 활용하여 최근 개발된 예측 디스플레이 기법을 적용, 효율적인 군집 로봇의 원격 제어가 가능하도록 하였다. 잘 알려진 논홀로노믹 패시브 디컴포지션 기법을 기반으로 대형 변경이 가능하도록 새로운 파라미터를 추가, 대형 변경간 발생할 수 있는 문제들에 대해 파악하고 이를 해결하기 위해 포텐셜 필드를 활용하였다. n대의 로봇으로 다양한 대형 변경이 가능토록 시뮬레이션 환경을 조성, 39대의 탱크를 이용하여여 5가지의 각기 다른 대형으로의 변환을 새로이 제시한 알고리즘을 적용하여 구현하였다. 또한 실제 로봇 3대를 활용하여 알고리즘의 효용성에 대한 실험을 필두로 좁은 길목, 개활지 등 연속적으로 변화하는 환경 속에서의 구동을 통해 최종적으로 제시한 프레임워크의 타당성에 대해 검증하였다.

주요어: Formation Reconfiguration, Nonholonomic Wheeled Mobile Robot, Passive Decomposition, Teleoperation

학번: *2017-22264*